JOURNAL OF GEOPHYSICAL RESEARCH, VOL. 113, D11110, doi:10.1029/2007JD009376, 2008

A new river flooding scheme for global climate applications: Off-line evaluation over South America

B. Decharme,[1] H. Douville,[1] C. Prigent,[2] F. Papa,[3] and F. Aires[4]

Received 11 September 2007; revised 15 January 2008; accepted 14 March 2008; published 6 June 2008.

[1] Given their strong interaction with both climate and the carbon cycle, wetlands and surface waters need to be parameterized in global general circulation models. For this purpose, a new simple flooding river scheme is proposed and evaluated over South America. The flood dynamics is described through the coupling between the ISBA land surface model and the TRIP river routing model including a prognostic flood reservoir. This reservoir fills when the river height exceeds a critical value and vice versa. The reservoir interacts with the soil hydrology through infiltration and with the overlying atmosphere through precipitation interception and free water surface evaporation. The model is tested in off-line mode using the 10-year ISLSCP-2 atmospheric forcing. The evaluation is made against satellite-derived inundation estimates as well as in situ river discharge observations. Besides a basin-scale increase in annual surface evaporation, the results show improved monthly discharges over the Amazon and Parana rivers, as well as a reasonable agreement between the simulated flooded areas and satellite-derived inundation estimates.

Citation: Decharme, B., H. Douville, C. Prigent, F. Papa, and F. Aires (2008), A new river flooding scheme for global climate applications: Off-line evaluation over South America, *J. Geophys. Res.*, *113*, D11110, doi:10.1029/2007JD009376.

1. Introduction

[2] Wetlands areas and inland water surfaces cover ~4–6% of the Earth's land surface [*Prigent et al.*, 2007]. At a coarse resolution and in first approximation, they can be separated in two categories: anthropogenic and natural. Manmade wetlands are associated with rice fields and agricultural irrigation while natural inundated areas are related to river flooding, lakes, marshes, and large ponds. All these wetlands are the world's largest source of methane [*Houweling et al.*, 1999; *Matthews*, 2000; *Bousquet et al.*, 2006] and could have contributed significantly to global warming since preindustrial time [*Shindell et al.*, 2004]. They have a strong influence on the annual cycle of river discharges in both tropical and high-latitude areas that also emphasize their relevance for water resource management. Finally, they affect the Earth's climate through their impact on the land surface water and energy budgets [*Krinner*, 2003]. Nevertheless, the lack of consistent data and techniques remains a major obstacle for characterizing their global variability. This situation has been improved recently with the various efforts to estimate surface water spatial and temporal dynamics [*Alsdorf et al.*, 2007]. For instance, using a multisatellite technique, *Prigent et al.* [2007] now offers the first global estimates of monthly inundation extents over almost a decade (1993–2000) and at a 0.25° horizontal resolution.

[3] Besides observations, the understanding of the wetlands interactions with climate, hydrology, and biochemistry requires numerical tools making it possible to analyze the mechanisms that control the extent or volume of the main wetland reservoirs and ultimately to predict their evolution from daily to climate change timescales. Recent efforts have been made to represent natural inland water surfaces in atmospheric general circulation models (AGCMs). Some studies use an implicit representation without any dedicated surface reservoir in order to estimate the potential feedback of wetland methane emissions on climate change [*Gedney et al.*, 2004]. Simple explicit parameterizations have been proposed, but they usually prescribe the residence time of water into predimensioned reservoirs [*Bonan*, 1995; *Coe*, 1998; *Krinner*, 2003] and are therefore not suitable for climate change studies. Except for big lakes, wetland reservoirs are not static in space-time and evolve with environmental and climate conditions, which is a key question regarding global warming since the methane emissions are mainly related to the wetland evolution [*Bousquet et al.*, 2006].

[4] The first goal of this study is to describe a new simple river flooding scheme for global climate and hydrological applications. The second objective is to assess the influence of seasonal floods on the simulated water budget over South America. South America has been selected because the main mechanism that controls the natural wetland dynamics

[1]Centre National de Recherche Météorologique, Météo-France, Toulouse, France.
[2]Laboratoire d'Etudes du Rayonnement et de la Matière en Astrophysique, Observatoire de Paris, Paris, France.
[3]NOAA Cooperative Remote Sensing Science and Technology Center, City College of New York, New York, New York, USA.
[4]Laboratoire de Météorologie Dynamique du CNRS/IPSL, Université Paris VI, Paris, France.

0148-0227/08/2007JD009376$09.00

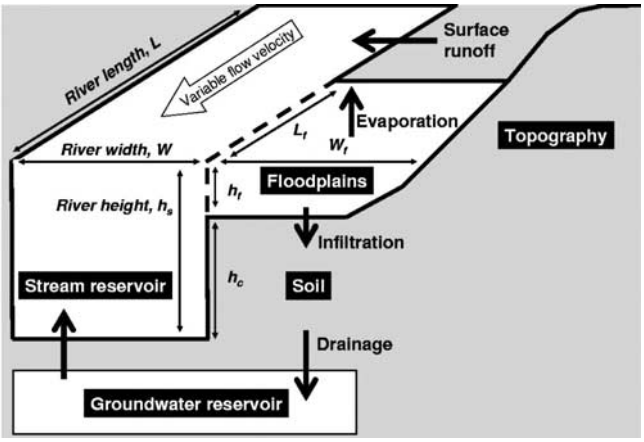

Figure 1. Schematic representation of the ISBA-TRIP coupled system. The surface runoff and the deep drainage flow into the stream and the groundwater reservoir, respectively. The stream reservoir has a rectangular geometry used to compute a variable velocity. The floodplains reservoir is cubic and defined by a width (W_f), a length (L_f), and a height (h_f). The surface evaporation, precipitation interception, and soil infiltration from the floodplains are explicitly represented. More details can be found in section 2.

is related to river flooding, which allows us to evaluate this preliminary scheme without the representation of lakes, marshes, and large ponds. It is important to note that this study is the first step of an attempt to represent the evolution of all inland water surfaces in AGCMs. The flooding scheme relies on the coupling between the Interaction Sol-Biosphère-Atmosphère (ISBA) land surface model (LSM) [*Noilhan and Planton*, 1989] and the Total Runoff Integrating Pathways (TRIP) river routing model (RRM) [*Oki and Sud*, 1998] (http://hydro.iis.u-tokyo.ac.jp/~taikan/TRIPDATA/TRIPDATA.html). The evaluation is made in off-line mode using the ISLSCP-2 global atmospheric forcing already used in the Global Soil Wetness Project [*Decharme and Douville*, 2007]. The simulations are evaluated against in situ river discharge measurements and satellite-derived inundation estimates from *Prigent et al.* [2007]. The river flooding scheme is presented in section 2. The experimental design, as well as these data, is described in section 3. Results are shown in section 4 while a discussion and the main conclusions are provided in sections 5 and 6, respectively.

2. River Flooding Scheme

[5] To represent river flooding, a simple coupling between ISBA and TRIP is proposed (Figure 1). ISBA is a relatively simple LSM that uses the force-restore method to calculate the time evolution of the surface energy and water budgets [*Noilhan and Planton*, 1989]. Recently, a comprehensive subgrid hydrology has been included in ISBA to account for the heterogeneity of precipitation, topography, and vegetation in each grid cell. A TOPMODEL approach [*Beven and Kirkby*, 1979] has been used to simulate a saturated fraction, f_{sat}, where precipitation is entirely converted into surface runoff (Dunne's mechanism) [*Decharme et al.*, 2006]. Infiltration (Horton's mechanism) is computed via two subgrid exponential distributions of rainfall intensity and soil maximum infiltration capacity. Finally, a tile approach is used to represent land cover and soil depth heterogeneities [*Decharme and Douville*, 2006a]. The TRIP RRM has been developed by *Oki and Sud* [1998] at the University of Tokyo. It is used at Météo-France to convert the simulated runoff into river discharge using a global river channel network at 1° resolution. The original TRIP model is based on a single prognostic reservoir whose discharge is linearly related to the river mass using a uniform and constant flow velocity. In the present study, a simple groundwater reservoir and a variable streamflow velocity have been added following *Arora and Boer* [1999] in which the variable velocity is computed using the water depth related to the stream water mass and assuming a rectangular river cross section. The prognostic equations for the groundwater reservoir, G (kg), and the stream reservoir, S (kg), are given by:

$$\left| \begin{array}{l} \dfrac{\partial G}{\partial t} = Q_{sb} - Q_{out}^{G} \\ \dfrac{\partial S}{\partial t} = \left(Q_{in}^{S} + Q_{out}^{G} + Q_{out}^{F}\right) - \left(Q_{in}^{F} + Q_{out}^{S}\right) \end{array} \right. \quad (1)$$

where Q_{sb} (kg s^{-1}) is the deep drainage simulated by ISBA. Q_{in}^{s} represents the sum of the surface runoff simulated by ISBA within the grid cell with the water inflow from the adjacent upstream neighboring grid cells and Q_{out}^{s} (kg s^{-1}) the grid cell discharge proportional to the variable streamflow velocity [*Arora and Boer*, 1999]. Q_{out}^{G} (kg s^{-1}) is the groundwater outflow proportional to a time-constant determined according to the dominant soil textural property into the grid cell [*Arora and Boer*, 1999]. Finally, Q_{in}^{F} and Q_{out}^{F} (kg.s^{-1}) represent the flood inflow and outflow, respectively.

[6] The floodplains are explicitly represented into the surface water and energy budgets computed by ISBA. The floodplain roughness length is estimated using the Charnock's formula, while the albedo of the surface free water varies with latitude [*Cogley*, 1979]. A new floodplain reservoir, F (kg), is introduced into TRIP within each grid cell of the hydrological network and linearly coupled with the stream reservoir:

$$\frac{\partial F}{\partial t} = Q_{in}^{F} + A\left(P_f - I_f - E_f\right) - Q_{out}^{F} \quad (2)$$

where A (m^2) is the grid area and P_f, I_f and E_f (kg m^{-2} s^{-1}) the precipitation interception by the floodplains, the reinfiltration, and the direct free water surface evaporation estimated by ISBA, respectively. I_f occurs if the flooded fraction, f_{flood}, is superior to f_{sat}, and depends on the soil maximum infiltration capacity. Floods arise when the water height of the stream reservoir is higher than the critical height of the river bed, h_c (Figure 2). This critical height varies linearly from the river mouth to the upstream

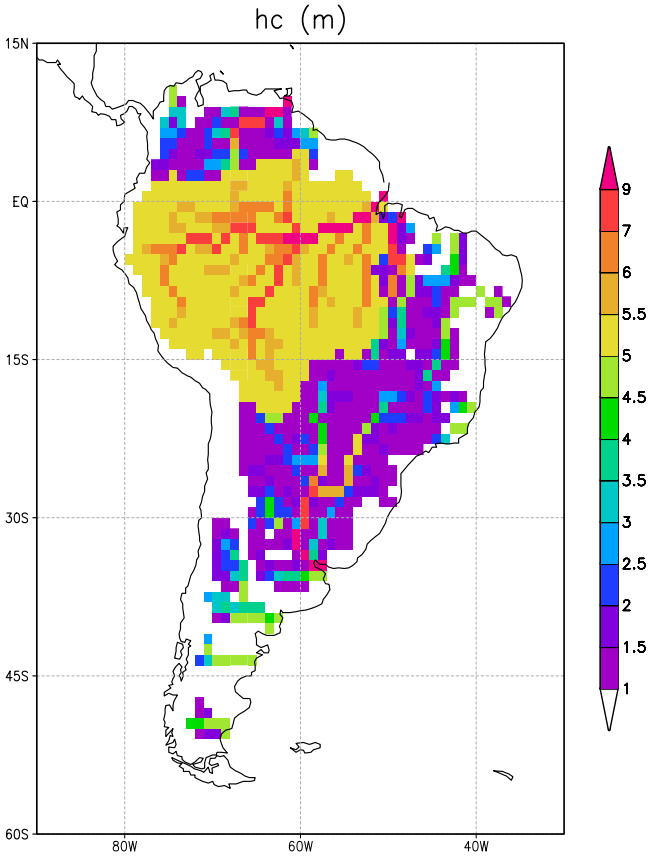

Figure 2. Spatial distribution of the critical height of the river bed, h_c (m), computed within the 1° by 1° hydrological network of the TRIP RRM. More details can be found in Appendix A.

regions of the basin. More details can be found in Appendix A.

3. Experimental Design and Data Sets

[7] The experimental design is similar to *Decharme and Douville* [2007]. An off-line hydrological simulation with the new flooding scheme (*Flood*) is compared to a control experiment without flooding (*CTL*). In addition, two sensitivity experiments to the h_c parameter are also performed using $h_c \pm 20\%$ globally. ISBA is integrated with a 5 min time step and coupled with TRIP once a day. Spin-up is performed using forcing data beginning 1 July 1982 and ending 31 December 1985, while the evaluation is made on the 1986–1995 period.

[8] Briefly, the meteorological forcing is the same as in the Global Soil Wetness Project (http://www.iges.org/gswp/). It covers more than 13 years (July 1982 to December 1995) at a 3-hourly time step and a 1° resolution. This data set is based on the National Center for Environmental Prediction/Department Of Energy (NCEP/DOE) reanalysis. Corrections to the systematic biases in the 3-hourly reanalyses are made by hybridization with global monthly climatologies [*Dirmeyer et al.*, 2006]. Note that the precipitation forcing used in this study is based on the P3 alternative product, presumed to be better than the B0 baseline product in which gauge undercatch has appeared to be overcorrected over middle and high latitudes [*Decharme and Douville*, 2006b]. The 10-year mean precipitation over the evaluation period (1986–1995) is given in Figure 3. The soil and vegetation parameters are specified according to the 1-km ECOCLIMAP database of Météo-France [*Masson et al.*, 2003]. The annual mean Leaf Area Index (LAI) and grid-cell mean topography over South

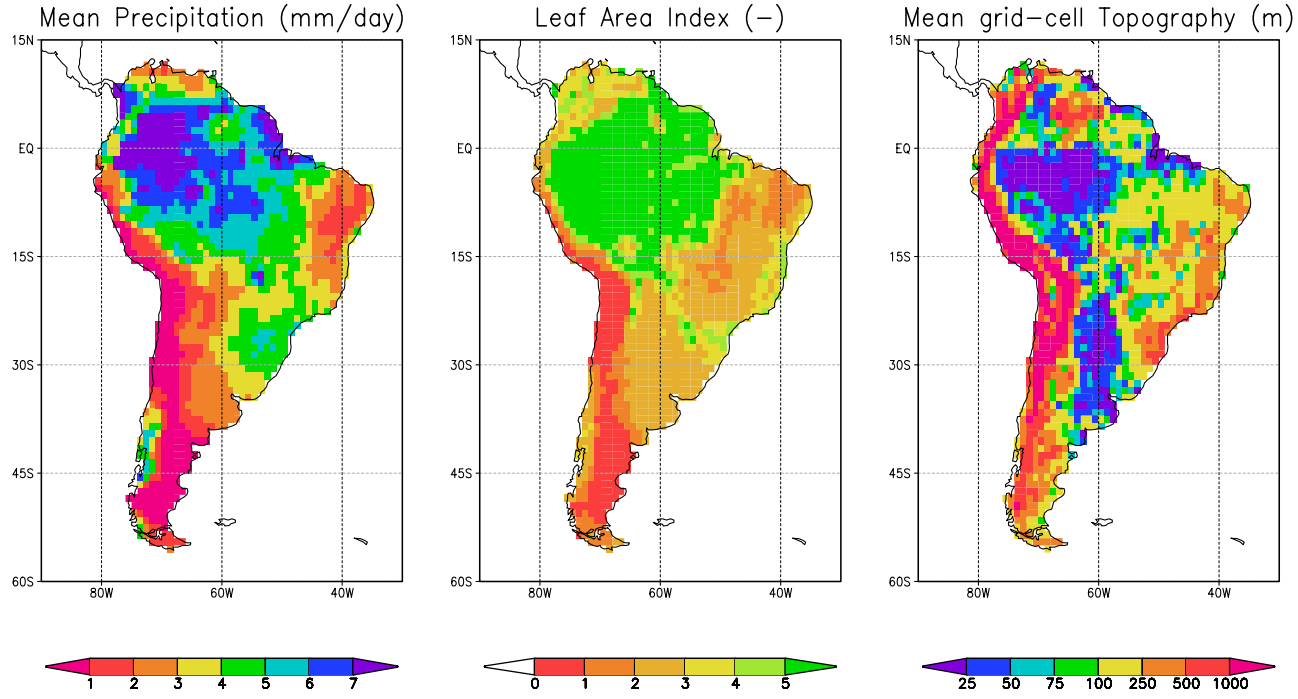

Figure 3. Ten-year mean precipitation (1986–1995) in mm/day and land surface characteristics over South America. The annual mean LAI (m^2/m^2) and the grid cell mean topography (m) are given.

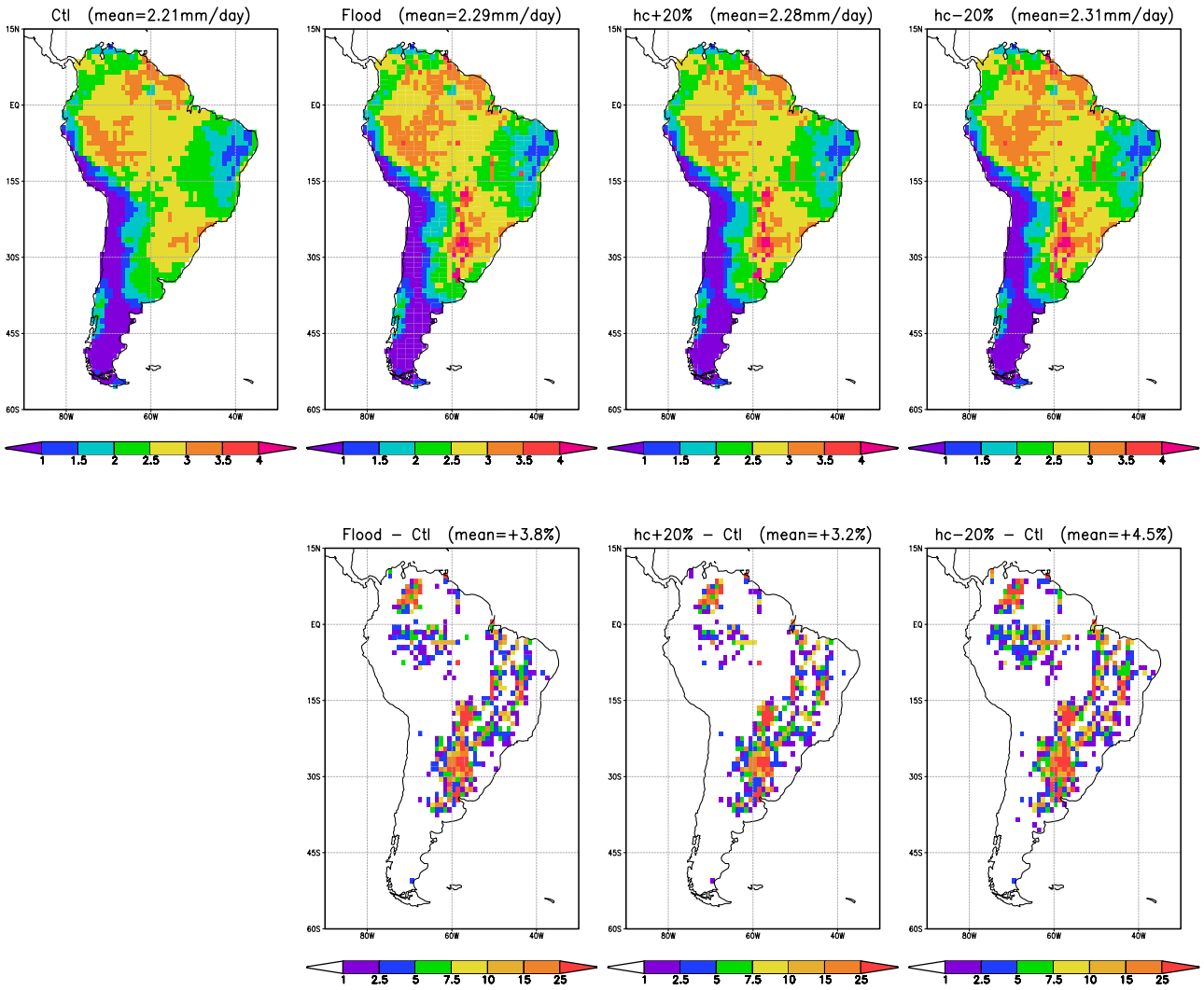

Figure 4. Spatial distribution expressed in mm d^{-1} and difference (in %) between the 10-year mean surface evaporation simulated by *CTL* and *Flood* experiments. The comparison between *CTL* and the sensitive experiments ($h_c \pm 20\%$) is also shown. Note that the mean value over the domain is given in the title of each picture.

America are also given in Figure 3. For the Amazonian equatorial forest (in the north), LAI exceeds 4 but is smaller over grassland and/or cropland areas.

[9] Over the evaluation period, the simulated discharges are compared to gauging measurements from the HyBAm data set (http://www.mpl.ird.fr/hybam/) for the Amazon and the Global Runoff Data Center (GRDC; http://www.grdc.sr.unh.edu/index.html) for the Parana. In addition, the satellite-derived inundation estimates from *Prigent et al.* [2007] are used to evaluate the spatial distribution and the time evolution of the simulated flooded fractions over the 1993–1995 period. This data set quantifies at the global scale the monthly variations of the distribution of surface water extent at ~25 km sampling intervals.

[10] It is derived from a complementary suite of satellite observations: Advanced Very High Resolution Radiometer (AVHRR) visible (0.58–0.68μm) and near-infrared (0.73–1.1μm) reflectances and the derived Normalized Difference Vegetation Index (NDVI); passive microwave emissivities between 19 and 85 GHz estimated from the Special Sensor Microwave/Imager (SSM/I) observations calculated as in the work of *Prigent et al.* [2006] by removing the contributions of the atmosphere (water vapor, clouds, rain) and the modulation by the surface temperature, using ancillary data from visible and infrared satellite observations from the International Satellite Cloud Climatology Project (ISCCP) [*Rossow and Schiffer*, 1999] and the NCEP reanalysis [*Kalnay et al.*, 1996]; and finally, backscatter at 5.25 GHz from the European Remote Sensing (ERS) satellite scatterometer. With the three sources of satellite data, an unsupervised classification is performed, and the pixels with satellite signatures likely related to inundations are retained. For each inundated pixel, the monthly fractional coverage by open water is the obtained using the passive microwave signal and a linear mixture model with end-members calibrated with scatterometer observations to account for the effects of vegetation cover. Global monthly mean surface water extent data set is created with a 0.25° spatial resolution at the equator and

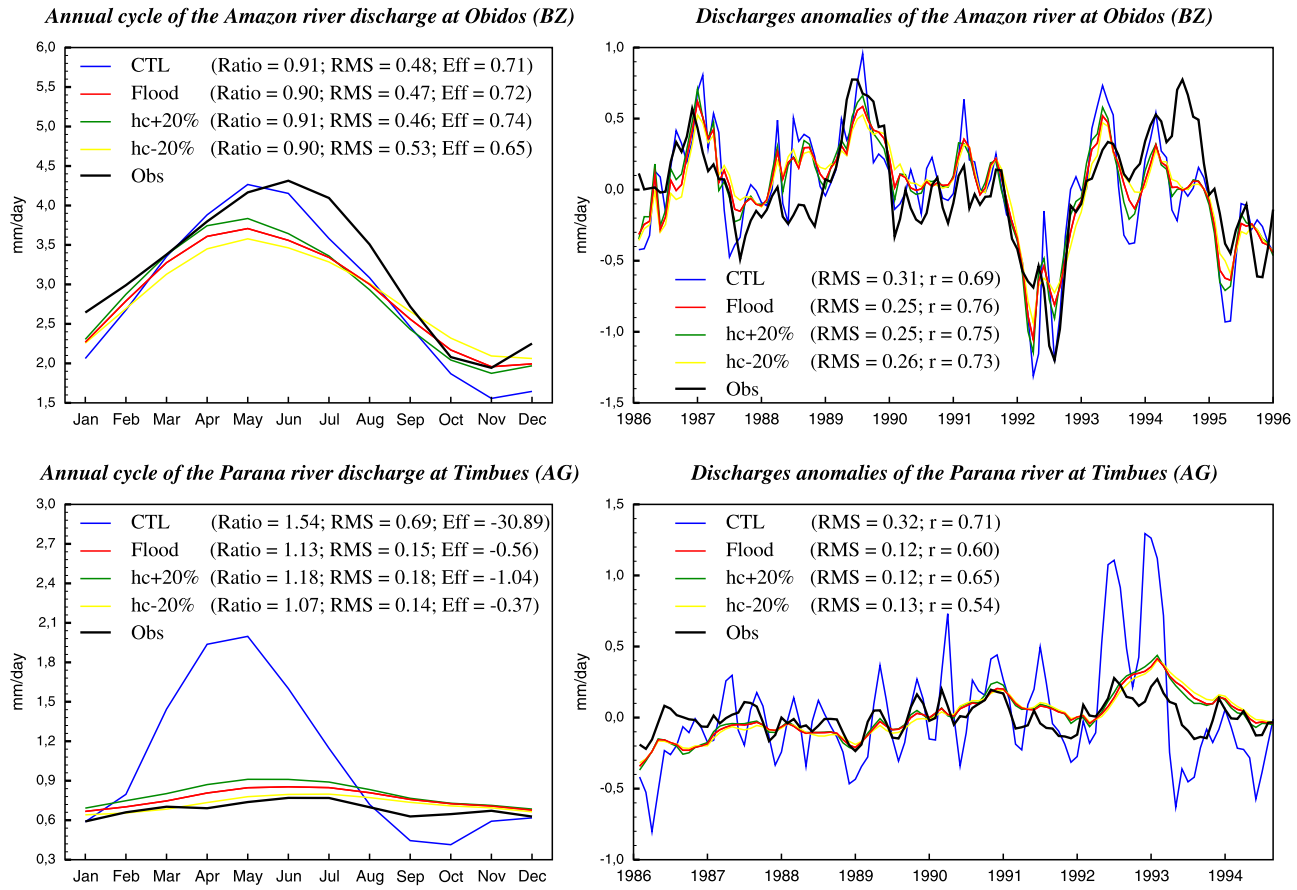

Figure 5. Mean annual cycle (left) and 10-year time series of monthly anomalies (right) of simulated and observed discharges over the (top) Amazon and the (bottom) Parana rivers basins. Simulations with (*Flood*) and without (*CTL*) the flooding scheme are presented as well as the sensitive experiments to h_c (±20%). Note that monthly efficiencies (*Eff*) shown on the left are calculated over the whole 10-year discharge observation period. The ratio between simulated and observed annual mean discharges (*Ratio*), as well as the root mean square error (*RMS*), is given. The correlation (r) between simulated and observed monthly anomalies is also shown.

is currently available for 1993–2000 [*Prigent et al.*, 2007; *Papa et al.*, 2006, 2007].

4. Results

[11] The comparison given in Figure 4 between the 10-year mean surface evaporation simulated by the *CTL* and *Flood* experiments shows that the introduction of the flooding scheme leads to a significant increase in surface evaporation, especially over the flat and herbaceous/cultivated regions of the Parana river basin (in the south). Over the Amazon, the increase is weaker since the direct evaporation from the free water surface is limited by the shading of the equatorial forest (cf. Appendix A). Note that the increase in surface evaporation is not very sensitive to the value of the h_c parameter.

[12] To evaluate these simulations, the simulated and observed discharges are compared over the Amazon and the Parana River basins. The simulated annual runoff is validated using the annual discharge ratio criterion (Ratio = $\overline{Q}_{sim}$ / $\overline{Q}_{obs}$), while the root mean square error (*RMS*), the correlation (r) and the efficiency (*Eff*) [*Nash and Sutcliffe*, 1970] criteria measure the model ability to capture the monthly discharge dynamics. This last skill score is defined as follows:

$$Eff = 1.0 - \frac{\sum \left(Q_{sim}(t) - Q_{obs}(t)\right)^2}{\sum \left(Q_{obs}(t) - \overline{Q_{obs}}\right)^2} \quad (3)$$

where $\overline{Q}_{obs}$ represents the observed temporal mean. *Eff* can be negative if the simulated discharge is very poor and is above 0.5 for a reasonable simulation. The mean annual cycles, as well as the monthly anomalies calculated over the whole observation period are represented in Figure 5. Over the Amazon, all scores are relatively insensitive to the flooding scheme, even if the anomaly correlation is appreciably enhanced. Conversely and in keeping with the stronger impact on surface evaporation, all discharge scores are significantly improved over the Parana. The only exception is the anomaly correlation that is slightly reduced, though the flooding scheme produces a realistic damping of the magnitude of the monthly discharge anomalies. Note also that the results are not very sensitive to the value of the h_c parameter, suggesting that our approach is relatively robust and that a 1-km topography might be sufficient to design an explicit river flooding scheme for global applications.

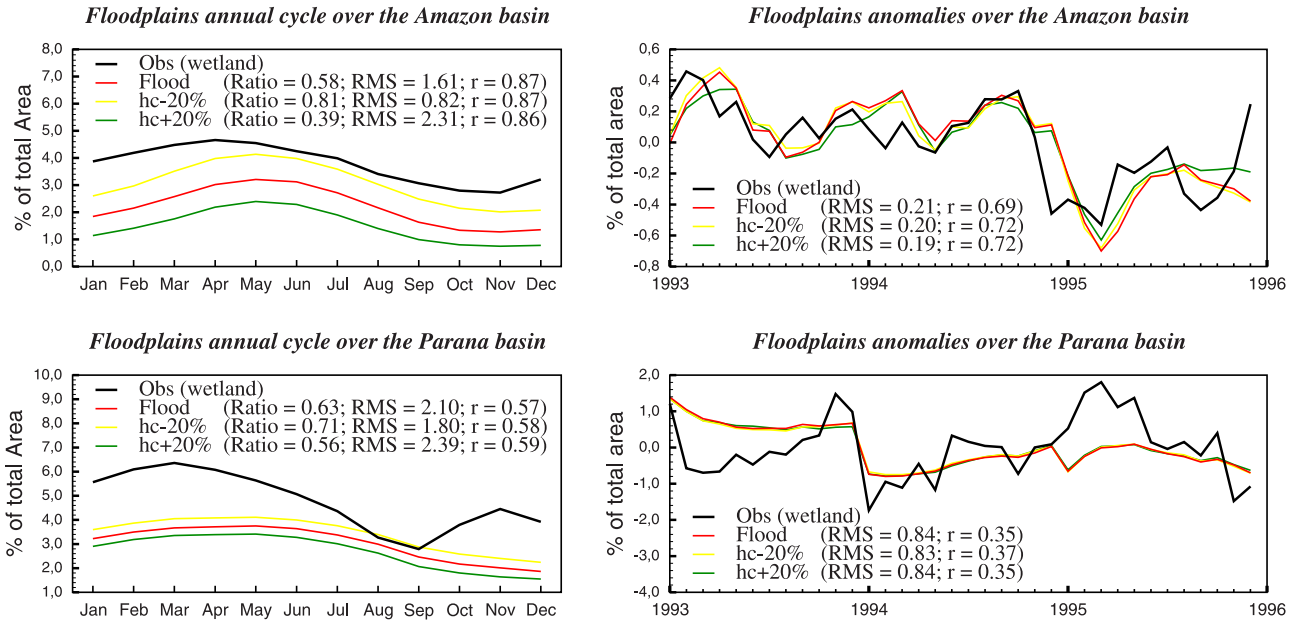

Figure 6. Comparison between simulated flooded fractions (*Flood*) and satellite-derived inundation estimates (*Obs*) over the Amazon and the Parana river basins during the 1993–1995 periods. The mean annual cycle and 3-year time series of monthly anomalies are shown in percent of the basin total area. All statistics are calculated over the whole 3-year period. Notations are the same than in Figure 4.

[13] Figures 6 to 8 compare the simulated flooded fractions to the satellite-derived inundation estimates from *Prigent et al.* [2007]. Basin-averaged annual cycles and monthly anomalies are shown for the Amazon and the Parana rivers (Figure 6). Over the Amazon, the mean annual cycle and the interannual variability are well captured even if the simulated flooded fractions seem to be underestimated. This bias is also found over the Parana where the monthly anomalies are less consistent with the satellite estimates than over the Amazon. The spatial distribution of the 3-year mean (1993–1995) simulated flooded fractions is also compared with the satellite data (Figure 7). The patterns are reasonable even if strong biases are found over flat and/or vegetated regions (as shown in Figure 3). Finally, the spatial display of the seasonal changes in simulated and satellite-derived flooded fraction extents is given in Figure 8. This figure shows that the bias found in Figure 7 is quasi similar over each season and the domain average values point out that the seasonal changes are appreciably reproduced.

[14] The sensitivity experiments indicate that a lower h_c value (−20% in this study) could reduce this basin-scale underestimation over the Amazon (Figure 6) but not for good reasons. This reduction is mainly due to a significant amplification of the overestimation of the simulated flooded fractions over the upstream part of the basin that is already shown in the *Flood* experiment (Figure 7). Over the Parana, the sensitivity to h_c is negligible. Indeed, the ratio between the mass of water available for flooding and the water mass in the streambed is more important than over the Amazon, as it is shown by the discharge ratio criterion with and without the flooding scheme (Figure 5). The h_c especially controls the maximum water mass in the streambed (Figure 1, Appendix A). Over the Parana, this maximum water mass is always less important than the potential mass of water inflowing or leaving the floodplains during the wet season and then the variations in h_c values appear negligible.

5. Discussion

[15] Our results suggest that the proposed simple flooding scheme improves the off-line simulation of the Amazon and Parana River discharges while providing a reasonable estimation of the variability of the inundated areas. Some aspects of the scheme are obviously questionable, such as the choice of the critical height of the river bed (h_c), the simplified geometry of the river stream and flood reservoirs, or the use of the Manning's formula for computing the mass transfer between them. Note however that the scheme is supposed to be used in global climate applications at a relatively low horizontal resolution (0.5° to 1°). Moreover, the sensitivity experiments with different values of h_c suggest that the model is relatively robust, without any particular tuning.

[16] As far as the annual mean water budget is concerned, the implementation of the flooding scheme leads to a clear reduction (from 54 to 13%) in the overestimation of the Parana discharge, while the Amazon discharge remains underestimated by 10%. Different reasons can account for such residual biases: deficiencies in the ISBA land surface model, uncertainties in the atmospheric forcing, and possible anthropogenic influence on the observed discharges [*Chapelon et al.*, 2002; *Fekete et al.*, 2004; *Ngo-Duc et al.*, 2005; *Decharme and Douville*, 2006b]. Another limitation is the resolution of the digital elevation model (DEM) which can induce an underestimation of the simulated flooded fraction through a failure to represent very flat regions or areas smaller than the horizontal and vertical resolution of the DEM [*Coe*, 1998]. In addition, satellite-

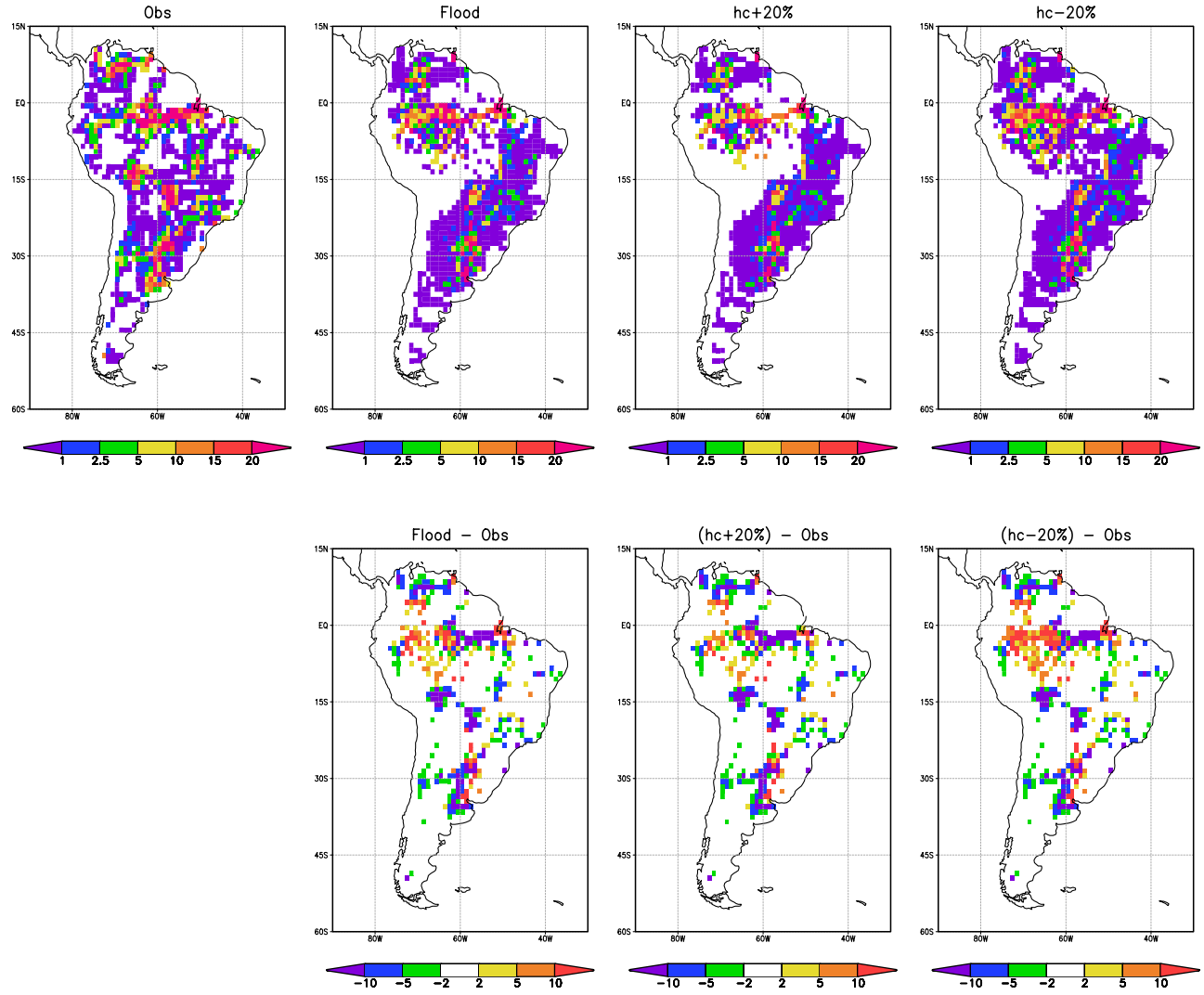

Figure 7. Spatial comparison between the 3-year mean simulated flooded fractions and satellite-derived inundation estimates (*Obs*) over South America. The *Flood* simulation as well as the sensitive experiments to h_c is shown.

derived inundation estimates could show some limitation, especially in densely vegetated areas [*Prigent et al.*, 2007].

[17] Nevertheless, the flooding scheme itself will need a more detailed validation, through an extension of the off-line simulations in both time (longer atmospheric forcings) and space (other river basins). Several assumptions will need to be tested more carefully such as the existence of a single floodplain in each grid cell and the use of a simplified geometry. Moreover, the strongest negative biases found in Figure 7 are mainly related to permanent open water areas (lakes or marshes) that are detected by the satellites but are not simulated by the flooding scheme. For example, *Martinez and Le Toan* [2007] have shown that these permanent water bodies are important in the downstream part of the Amazon basin, in which the flooded fractions are indeed underestimated by our model.

6. Conclusion

[18] This study describes an original river flooding scheme for global hydrological and climate applications. The model is based on the coupling between the ISBA land surface model, in which a flooded fraction has been defined, and the TRIP river routing model, in which a flood reservoir has been introduced. It is tested over South America where seasonal floods have a clear influence on the observed river discharges, using off-line simulations at a 1° by 1° resolution driven by the 1986–1995 ISLSCP-2 atmospheric forcing. The flooding scheme accounts explicitly for the precipitation interception by the floodplains, the direct evaporation from the free water surface and the possible reinfiltration into the soil. The simulated river discharges are evaluated against in situ gauging measurements over the Amazon and the Parana rivers basins, while the simulated flooded areas are compared to satellite-derived inundation estimates from *Prigent et al.* [2007].

[19] The implementation of this scheme leads to an increase in surface evaporation (especially over Parana) and thus affects the land surface water and energy budgets at the daily to interannual timescales. Such processes are expected to have significant regional impacts on climate

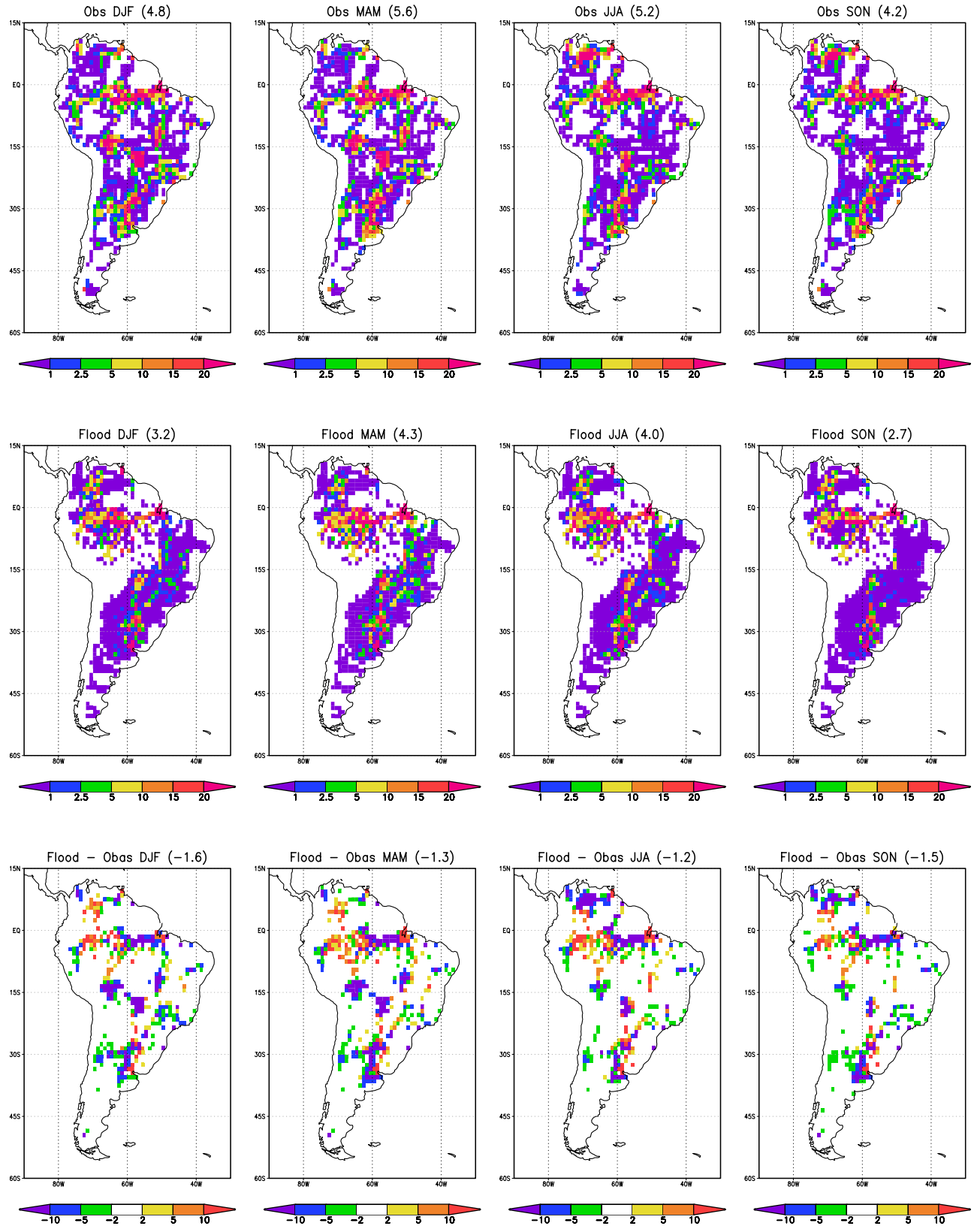

Figure 8. Spatial display of the seasonal changes in flood extent (in percent) for both (top) the satellite-derived inundation estimates and (middle) the *Flood* simulation. The domain average values (in percent of the total surface) are given in each title panel for each season: winter (DJF), spring (MAM), summer (JJA), and autumn (SON). (bottom) The seasonal biases are also shown.

variability and the ultimate objective will be to introduce this ISBA-TRIP coupled hydrology in the CNRM global climate model. Nevertheless, the scheme will first need to be further validated in off-line mode. The positive impacts found on the simulated Parana and Amazon River discharges will have to be confirmed over other large river basins using an extended atmospheric forcing such as the global 1948–2000 data set of *Sheffield et al.* [2006]. Further improvements could be made by adding an explicit representation of lakes, marshes, and large ponds. In addition, the treatment of groundwater in TRIP could be considerably improved by using a two-dimensional approach where the water flux between the groundwater and ISBA or the stream reservoir as well as the water exchange between each neighboring grid cell could be explicitly calculated [*Fan et al.*, 2007; *Miguez-Macho et al.*, 2007]. Finally, the flooding scheme could be coupled to a biogeochemical scheme in order to simulate the natural emissions of methane and their possible sensitivity to global climate change, either in off-line or coupled mode.

Appendix A: Flooding River Scheme

[20] As for the stream reservoir, a rectangular geometry is assumed to represent the floodplain reservoir in each grid cell. The flood outflow, Q_{out}^{F} (kg s^{-1}), and inflow, Q_{int}^{F} (kg s^{-1}), from this reservoir (equation (1)) are given by:

$$Q_{in}^{F} = \frac{v_{in}}{W + W_f} M_f \tag{A1}$$

$$Q_{out}^{F} = \frac{v_{out}}{W + W_f}\left[\delta F + (1-\delta)\max\left(0, M_f\right)\right] \left| \begin{array}{l} \delta = 0 \forall F > M_f \\ \delta = 1 \forall F \le M_f \end{array} \right. \tag{A2}$$

where F (kg) is the water mass in the floodplain reservoir, W_f (m) is the floodplain width, and M_f (kg), in absolute value, is the potential mass of water inflowing (positive M_f) or leaving (negative M_f) the floodplain reservoir assuming an equilibrium state between the stream and the floodplain water depth:

$$M_f = \rho_w L_f W\left(h_s - h_c - h_f\right) \tag{A3}$$

where ρ_w (kg m^{-3}) is the water density, L_f (m) and h_f (m) are the length and the depth of the floodplains, h_s (m) is the water height of the stream reservoir, h_c (m) is the critical height of the river bed, and W (m) is the stream river width. W is estimated at each river cross section using a geomorphologic relationship and then varies from the river mouth to the upstream grid cells [*Arora and Boer*, 1999]. $W+W_f$ represents the distance covered by M_f from the stream to the floodplains or conversely. Here v_{in} and v_{out} (m s^{-1}) are the flood inflow and outflow velocities computed using the Manning's formula:

$$v = \frac{\sqrt{s_f}}{n_f} R_f^{2/3} \tag{A4}$$

where $n_f = 0.1$ is the Manning roughness coefficient for the floodplains while s_f (m m^{-1}) and R_f (m) are the slope and the hydraulic radius respectively at the interface between the floodplain and the river stream:

$$R_f = \frac{L_f\left|\max(0, h_s - h_c) - h_f\right|}{L_f + 2\left|\max(0, h_s - h_c) - h_f\right|} \tag{A5}$$

$$s_f = \frac{\left|\max(0, h_s - h_c) - h_f\right|}{W + W_f} \tag{A6}$$

where h_f is calculated with the help of the actual distribution of the elevation in each grid cell. The elevation, E (m), is available at a 1 km by 1 km resolution using the HYDRO1K data set (http://edcdaac.usgs.gov/gtopo30/hydro). For each pixel i, a local height, h_i (m), is calculated according to $h_i = E_i - E_{\min}$ where $E_{\min}$ is the grid cell minimum elevation. Therefore, for each h_i associated with a fraction, f_i, of the grid cell, a potential volume of flood, $V(h_i)$ (kg), can be simply calculated as follows:

$$V(h_i) = \rho_w\left(A\sum_{0}^{i} f_i\right)\left(h_i - \frac{\sum_{0}^{i} h_i f_i}{\sum_{0}^{i} f_i}\right) \tag{A7}$$

The flooded fraction, f_{flood}, can be estimated at each time step and in each grid cell by comparison between the water volume into the floodplain reservoir, F, computed by TRIP (equation (1)) and this potential volume $V(h_i)$:

$$F = V(h_i) \Rightarrow f_{flood} = \sum_{0}^{i} f_i \tag{A8}$$

So, h_f, W_f, and L_f within the grid cell ca be simply calculated as follows:

$$\left| \begin{array}{l} h_f = \dfrac{F}{\rho_w A f_{flood}} \\ L_f = \max\left(0.01L,\ r\sqrt{f_{flood}A}\right) \\ W_f = \dfrac{A f_{flood}}{L_f} \end{array} \right. \tag{A9}$$

where r is the meandering ratio fixed to 1.4 as recommended by *Oki and Sud* [1998]. Here h_c varies linearly with the river width and it is simply computed in each grid cell as follows:

$$h_c = (h_{\min} - h_{\max})\frac{W_{mouth} - W}{W_{mouth} - W_{\min}} + h_{\max} \tag{A10}$$

where $h_{\min}$ (m) and $h_{\max}$ (m) are the minimum and the maximum river bed height over the basin, respectively. W_{mouth} (m) and $W_{\min}$ (m) are the river width at the river mouth and at the upstream grid cell over the basin, respectively. Here

h_{min} = 1 m if W_{min} < 500 m and 5 m elsewhere while h_{max} = 5 m if W_{mouth} < 1000 m and 10 m elsewhere (Figure 2). Note that this empirical formulation (equation (A10)) leads to a drastic sharp transition in h_c value at the basin boundary, especially in the upstream part of the Amazon. This fact could be improved by using a nonlinear function and by adding information on the distance to the river mouth.

[21] Finally, because ISBA uses a single surface temperature, a new fraction, p_{ff}, is added in each grid cell to account for the effect of the floodplains on the surface energy budget. A fraction of vegetation masked by the floodplains, $p_{f,veg}$, is first estimated and is combined with the TRIP flooded fraction, f_{flood}, as follows:

$$\begin{cases} p_{f,veg} = \min\left[\frac{h_f}{h_f + h_{veg}}, f_{flood}\right] \\ p_{ff} = (1 - veg) f_{flood} + veg\ p_{f,veg} \end{cases} \quad \text{(A11)}$$

where h_{veg} (m) and veg are the height and the fraction of the vegetation, respectively. According to the ECOCLIMAP database, h_{veg} = z_0/0.13 where z_0 (m) is the vegetation roughness length. Then, the direct evaporation from this flooded fraction is simply estimated by:

$$E_f = p_{ff} \rho_a C_H V_a [q_{sat}(T_s, P_s) - q_a] \quad \text{(A12)}$$

where ρ_a is the air density, q_a is the air humidity, V_a is the wind speed, C_H is the drag coefficient depending upon the thermal stability of the atmosphere, and q_{sat} is the saturated specific humidity that depends on surface temperature, T_s, and pressure, P_s.

[22] **Acknowledgments.** The authors would like to thank all French and Brazilian teams that contribute to the HyBam data set and particularly the IRD (Institut pour la Recherche et le Développement). Thanks are also due to the anonymous reviewers for their constructive comments. This work was supported by Météo-France/CNRM (Centre National de Recherche Météorologique) and by the CNRS (Centre National de la Recherche Scientifique) of the French Research Ministry.

References

Alsdorf, D. E., E. Rodrýguez, and D. P. Lettenmaier (2007), Measuring surface water from space, *Rev. Geophys.*, *45*, RG2002, doi:10.1029/2006RG000197.

Arora, V. K., and G. J. Boer (1999), A variable velocity flow routing algorithm for GCMs, *J. Geophys. Res.*, *104*, 30,965–30,979, doi:10.1029/1999JD900905.

Beven, K. J., and M. J. Kirkby (1979), A physically-based variable contributing area model of basin hydrology, *Hydrol. Sci. Bull.*, *24*, 43–69.

Bonan, G. B. (1995), Sensitivity of a GCM to inclusion of inland water surfaces, *J. Clim.*, *8*, 2691–2704, doi:10.1175/1520-0442(1995)008<2691:SOAGST>2.0.CO;2.

Bousquet, P., et al. (2006), Contribution of anthropogenic and natural sources to atmospheric methane variability, *Nature*, *443*, 439–443, doi:10.1038/nature05132.

Chapelon, N., H. Douville, P. Kosuth, and T. Oki (2002), Off-line simulation of the Amazon water balance: A sensitivity study with implications for GSWP, *Clim. Dyn.*, *19*, 141–154, doi:10.1007/s00382-001-0213-9.

Coe, M. (1998), A linked global model of terrestrial processes: Simulation of modern rivers, lakes and wetlands, *J. Geophys. Res.*, *103*, 8885–8899, doi:10.1029/98JD00347.

Cogley, J. G. (1979), The albedo of water as a function of latitude, *Mon. Weather Rev.*, *107*, 775–781, doi:10.1175/1520-0493(1979)107<0775:TAOWAA>2.0.CO;2.

Decharme, B., and H. Douville (2006a), Introduction of a sub-grid hydrology in the ISBA land surface model, *Clim. Dyn.*, *26*, 65–78, doi:10.1007/s00382-005-0059-7.

Decharme, B., and H. Douville (2006b), Uncertainties in the GSWP-2 precipitation forcing and their impacts on regional and global hydrological simulations, *Clim. Dyn.*, *27*, 695–713, doi:10.1007/s00382-006-0160-6.

Decharme, B., and H. Douville (2007), Global validation of the ISBA Sub-Grid Hydrology, *Clim. Dyn.*, *29*, 21–37, doi:10.1007/s00382-006-0216-7.

Decharme, B., H. Douville, A. Boone, F. Habets, and J. Noilhan (2006), Impact of an exponential profile of saturated hydraulic conductivity within the ISBA LSM: Simulations over the Rhone basin, *J. Hydrometeorol.*, *7*, 61–80, doi:10.1175/JHM469.1.

Dirmeyer, P. A., X. Gao, M. Zhao, Z. Guo, T. Oki, and N. Hanasaki (2006), The Second Global Soil Wetness Project (GSWP-2), Multi-model analysis and implications for our perception of the land surface, *Bull. Am. Meteorol. Soc.*, *87*, 1381–1397, doi:10.1175/BAMS-87-10-1381.

Fan, Y., G. Miguez-Macho, C.-P. Weaver, R. Walko, and A. Robock (2007), Incorporating water table dynamics in climate modeling: 1. Water table observations and equilibrium water table simulations, *J. Geophys. Res.*, *112*, D10125, doi:10.1029/2006JD008111.

Fekete, B. M., C. J. Vörösmarty, J. O. Road, and C. J. Willmott (2004), Uncertainties in precipitation and their impacts on runoff estimates, *J. Clim.*, *17*, 294–304, doi:10.1175/1520-0442(2004)017<0294:UIPATI>2.0.CO;2.

Gedney, N., P. M. Cox, and C. Huntingford (2004), Climate feedback from wetland methane emission, *Geophys. Res. Lett.*, *31*, L20503, doi:10.1029/2004GL020919.

Houweling, S., T. Kaminski, F. Dentener, J. Lelieveld, and M. Heinmann (1999), Inverse modeling of methane sources and sinks using adjoint of a global transport model, *J. Geophys. Res.*, *104*, 26,137–26,160, doi:10.1029/1999JD900428.

Kalnay, E., et al. (1996), The NCEP/NCAR 40-year reanalysis project, *Bull. Am. Meteorol. Soc.*, *77*, 437–470, doi:10.1175/1520-0477(1996)077<0437:TNYRP>2.0.CO;2.

Krinner, G. (2003), Impact of lakes and wetlands on boreal climate, *J. Geophys. Res.*, *108*(D16), 4520, doi:10.1029/2002JD002597.

Martinez, J. M., and T. Le Toan (2007), Mapping of flood dynamics and spatial distribution of vegetation in the Amazon floodplain using multitemporal SAR data, *Remote Sens. Environ.*, *108*, 209–223, doi:10.1016/j.rse.2006.11.012.

Masson, V., J. L. Champeaux, F. Chauvin, C. Mériguet, and R. Lacaze (2003), A global database of land surface parameters at 1km resolution for use in meteorological and climate models, *J. Clim.*, *16*, 1261–1282.

Matthews, E. (2000), Wetlands, in *Atmospheric Methane: Its Role in the Global Environment*, edited by M. A. K. Khalil, pp. 202–233, Springer, New York.

Miguez-Macho, G., Y. Fan, C.-P. Weaver, R. Walko, and A. Robock (2007), Incorporating water table dynamics in climate modeling: 2. Formulation, validation, and soil moisture simulation, *J. Geophys. Res.*, *112*, D13108, doi:10.1029/2006JD008112.

Nash, J. E., and J. V. Sutcliffe (1970), River flow forecasting through conceptual models, 1. A discussion of principles, *J. Hydrol. Amsterdam*, *10*, 282–290, doi:10.1016/0022-1694(70)90255-6.

Ngo-Duc, T., J. Polcher, and K. Laval (2005), A 53-year forcing data set for land surface models, *J. Geophys. Res.*, *110*, D06116, doi:10.1029/2004JD005434.

Noilhan, J., and S. Planton (1989), A simple parameterization of land surface processes for meteorological models, *Mon. Weather Rev.*, *117*, 536–549, doi:10.1175/1520-0493(1989)117<0536:ASPOLS>2.0.CO;2.

Oki, T., and Y. C. Sud (1998), Design of Total Runoff Integrating Pathways (TRIP), A global river channel network, *Earth Interact.*, *2*, 1–36, doi:10.1175/1087-3562(1998)002<0001:DOTRIP>2.3.CO;2.

Papa, F., C. Prigent, F. Durand, and W. B. Rossow (2006), Wetland dynamics using a suite of satellite observations: A case study of application and evaluation for the Indian Subcontinent, *Geophys. Res. Lett.*, *33*, L08401, doi:10.1029/2006GL025767.

Papa, F., C. Prigent, and W. B. Rossow (2007), Ob' River flood inundations from satellite observations: A relationship with winter snow parameters and river runoff, *J. Geophys. Res.*, *112*, D18103, doi:10.1029/2007JD008451.

Prigent, C., F. Aires, and W. B. Rossow (2006), Land surface microwave emissivities over the globe for a decade, *Bull. Am. Meteorol. Soc.*, *87*, 1573–1584, doi:10.1175/BAMS-87-11-1573.

Prigent, C., F. Papa, F. Aires, W. B. Rossow, and E. Matthews (2007), Global inundation dynamics inferred from multiple satellite observations, 1993–2000, *J. Geophys. Res.*, *112*, D12107, doi:10.1029/2006JD007847.

Rossow, W. B., and R. A. Schiffer (1999), Advances in understanding clouds from ISCCP, *Bull. Am. Meteorol. Soc.*, *80*, 2261–2287, doi:10.1175/1520-0477(1999)080<2261:AIUCFI>2.0.CO;2.

Sheffield, J., G. Goteti, and E. Wood (2006), Development of a 50-yr high resolution global dataset of meteorological forcings for land surface modeling, *J. Clim.*, *19*, 3088–3111, doi:10.1175/JCLI3790.1.

Shindell, D. T., G. Falugevi, N. Bell, and G. A. Schmidt (2004), An emission-based view of climate forcing by methane and tropospheric ozone, *Geophys. Res. Lett.*, *32*, L04803, doi:10.1029/2004GL021900.

F. Aires, Laboratoire de Météorologie Dynamique du CNRS/IPSL, Université Paris VI, 4, place Jussieu, F-75252 Paris, France.

B. Decharme and H. Douville, Centre National de Recherche Météorologique, Météo-France, 42 avenue G. Coriolis, F-31057 Toulouse, France. (bertrand.decharme@cnrm.meteo.fr)

F. Papa, NOAA Cooperative Remote Sensing Science and Technology Center, City College of New York, New York, NY 10031, USA.

C. Prigent, Laboratoire d'Etudes du Rayonnement et de la Matière en Astrophysique, Observatoire de Paris, 61 avenue de l'Observatoire, F-75014 Paris, France.